Approaches to Wave Packet Imaging Using Femtosecond Ionization Spectroscopy†

S. Gräfe, D. Scheidel, and V. Engel*

Institut für Physikalische Chemie, Universität Würzburg, Am Hubland, D-97074 Würzburg, Germany

N. E. Henriksen and K. B. Møller

Department of Chemistry, Technical University of Denmark, DTU 207, DK-2800 Lyngby, Denmark

Received: March 18, 2004

Different methods to obtain information about the probability densities of vibrational wave packets in diatomic molecule are compared. More explicitly, we consider pump−probe ionization processes. Time-resolved photoelectron spectra and total ion yields as well as fragment ion distributions are calculated, and these different quantities are employed to reconstruct radial densities. It is shown that pump−probe ionization experiments are well suited for the mapping of vibrational wave packets.

1. Introduction

The preparation of quantum mechanical wave packets and the real-time observation of their dynamics is at the heart of time-resolved spectroscopy with femtosecond laser pulses.[1,2] In a typical experiment, a first laser pulse, commonly termed the pump pulse, interacts with the system and produces a linear combination of eigenstates, i.e., a wave packet. At a variable delay-time a second pulse (probe) causes another transition in the system. A signal then is recorded as a function of the pump−probe delay, yielding information about the dynamical behavior of the system under investigation. Here we are concerned with pump−probe ionization measurements where the transient signal consists of an ion yield or photoelectron distribution. Many experiments have been performed using femtosecond pump−probe ionization and the detection of ions, see, e.g., refs 3−6. Also, femtosecond time-resolved photoelectron spectroscopy, which has been reviewed extensively recently,[7−9] has become a valuable technique to investigate dynamical processes in molecules.

The present paper is concerned with pump−probe ionization signals and the imaging of molecular wave packets. To be more precise, the question to be asked is as follows: if a vibrational wave packet is prepared in a molecule, then how much of the properties of this packet can be traced in a signal? The relation of measured signals to quantum mechanical wave functions has a long history. As a prominent example, we mention the reflection principle of cw-spectroscopy: in a molecular bound-to-free transition, the absorption spectrum directly reflects the ground-state wave function of the system;[10−12] for an application in atomic photoionization, see the work of Rost.[13] Likewise, excitation profiles in continuum resonance Raman spectroscopy map the nodal structure of the final state in the two-photon process.[14−17] Also, it is possible to relate properties of wave functions directly to rotational (rotational reflection principle[18]) and vibrational (vibrational reflection principle[19]) fragment distributions in photodissociation processes.

Whereas the latter examples do not explicitly involve time, i.e., transient changes of a system, the imaging of wave packets in time-resolved experiments has been addressed by several groups. It is, for example, possible to use the technique of time-gated emission spectroscopy[20] to map the probability density of vibrational wave packets in a diatomic molecule.[21,22] Also, it can be shown that the probability density of a wave packet which serves as the initial state for a resonant excitation of a molecule in a well defined geometry can be related to the time-derivative of a pump−probe fluorescence signal.[23,24]

Regarding ionization processes, other approaches have been realized. Seel and Domcke showed that time-resolved photoelectron spectra directly reflect the wave packet dynamics in molecules.[25,26] Their seminal study treated a multi-mode vibrational dynamics in pyracine but the mapping is unique in the simple case of a single vibrational mode, e.g. for a diatomic molecule.[27] Here, femtosecond experiments of Baumert and coworkers showed beautifully the changes of radial probability densities in the Na_2 molecule in weak[28] and strong laser fields.[29,30] Another technique employs Coulomb explosion of molecules where dissociating ions interact via their pure Coulomb repulsion.[31−33] Here, the asymptotic momentum distribution yields information about the wave packet in the neutral system. Of course, this technique can also be applied to ionization processes involving single or double ionization.[34,35]

Experimental and theoretical efforts have been reported which aim at the construction of wave packets, concerning not only their density but also their phase.[22,36−40] This topic will not be discussed here.

In the following sections, we investigate the vibrational motion in a bound-state potential of the sodium dimer (see Figure 1). The probe pulse initiates a transition to an antibonding state of the cationic molecule. We calculate the transient signals of photoelectron spectra, total ion yields, and fragment momentum distributions and compare quantum mechanical densities as constructed from the various signals with the numerically obtained ones. The theory and the model are described in section 2. Numerical results are presented in section 3 and a summary is given in section 4.

2. Theory and Model

2.1. Pump—Probe Ionization. We regard a pump/probe process involving three electronic states. In our numerical example, these states correspond to the electronic ground-state

† Part of the "Gert D. Billing Memorial Issue".

* Corresponding author. Telephone: +49-931-888-6376. Fax: +49-931-888-6362. E-mail: voen@phys-chemie.uni-wuerzburg.de.

10.1021/jp040230q CCC: $27.50 © 2004 American Chemical Society
Published on Web 07/29/2004

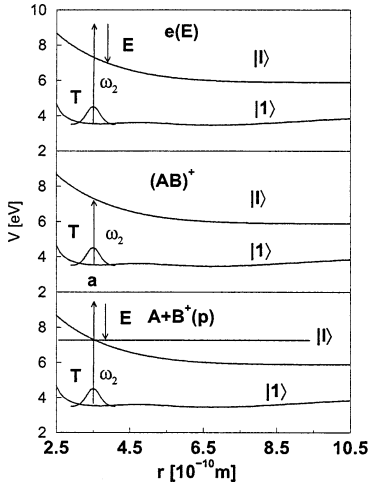

Figure 1. Pump−probe ionization schemes. Upper panel: ionization at a delay-time T yielding photoelectrons with different kinetic energies E. Middle panel: threshold ionization with different photon energies (indicated by the arrows) allowing one to image properties of the vibrational wave packet passing a critical bond length $a(T)$ where ionization becomes possible. Lower panel: during an ionization at delay-time T, building of fragments with momenta p. This goes in hand with the production of photoelectrons with energy E. The horizontal line defines an energy ϵ corresponding to a kinetic fragment energy of $\epsilon - V_I(\infty) = p^2/(2m)$.

$|0\rangle$ ($^1\Sigma_g^+$), the double minimum state $|1\rangle$ ($^1\Sigma_u^+$) and the dissociative ionic state $|I\rangle$ ($^2\Sigma_u^+$) of the sodium dimer. The potentials of the latter two states are displayed in Figure 1. In the pump process, initiated by a femtosecond pulse with a photon energy of ω_1 (atomic units are used throughout this paper), a vibrational wave packet is prepared in state $|1\rangle$. Within the probe transition (ω_2), ionization takes place at a defined delay-time T. The ionization scheme, as displayed in Figure 1, was realized in several femtosecond pump−probe ionization experiments.[34,41−43]

In what follows, we assume that all transitions are electric dipole transitions and the fields are weak so that the matter−light interaction may be described by time-dependent perturbation theory. Thus, the wave packet prepared in the pump process can be written as

$$|\psi_1(t)\rangle = U_1(t)|\psi_1(0)\rangle \tag{1}$$

where $U_1(t)$ is the propagator for the nuclear motion in state $|1\rangle$ and

$$|\psi_1(0)\rangle = \frac{1}{i}\int_{-\infty}^{+\infty} \mathrm{d}t\, U_1(-t)\, W_1(t)\, U_0(t)|\psi_0\rangle \tag{2}$$

Here $|\psi_0\rangle$ is the initial vibrational state in the electronic ground state $|0\rangle$ (the rotational motion is not included in what follows), evolving in time with the nuclear propagator $U_0(t)$. The interaction energy is

$$W_1(t) = -\frac{1}{2}\mu_{10}\, g_1(t)\, \mathrm{e}^{-i\omega_1 t} \tag{3}$$

where only the term leading to absorption was kept. The pulse envelope is denoted as $g_1(t)$ and μ_{10} is the projection of the transition dipole moment on the field polarization vector.

The wave packet $|\psi_1(t)\rangle$ moves unperturbed until the second laser pulse starts interacting with the molecular sample at time T, thus inducing ionization. In the ionization process, the photon energy is shared between the photoelectron and cationic molecule. The wave function corresponding to the ejection of a photoelectron with kinetic energy E then is[25,26]

$$|\psi_E(t)\rangle = U_E(t - T)\, |\psi_E(T)\rangle \tag{4}$$

with

$$|\psi_E(T)\rangle = \frac{1}{i}\int_{-\infty}^{+\infty} \mathrm{d}t\, U_E(-t)\, W_2(t)\, U_1(t)\, |\psi_1(T)\rangle \tag{5}$$

Here, we assumed (besides the usual Born−Oppenheimer separation of electronic and nuclear degrees-of-freedom) that the photoelectron decouples from the nuclei and the other electrons. The propagator in the ionic state, $U_E(t) = \exp[-i(H_I + E)t]$, contains the nuclear Hamiltonian H_I and the photoelectron energy as an additive constant. The interaction energy is

$$W_2(t) = -\frac{1}{2}\mu_{I1}\, g_2(t)\, \mathrm{e}^{-i\omega_2 t} \tag{6}$$

where the notation is as above.

The states $|\psi_E(t)\rangle$ are of central importance for the calculation of various experimentally accessible signals as will be detailed in the next subsection. To calculate these states we solve the time-dependent Schrödinger equation using the method of Feit and Fleck.[44] The ionization continuum is discretized so that the nuclear ionic wave function is calculated for a finite number of energies E_n. All transition dipole moments are, within the Condon approximation, set to a constant value of $\mu_{nm} = 1$.

2.2. Pump—Probe Ionization Signals. The photoelectron spectrum $P(E, T)$ is determined from the probability of finding electrons with a fixed kinetic energy E which is given as the norm of the ionic states of eq 5:

$$P(E, T) = \langle\psi_E(T)|\psi_E(T)\rangle \tag{7}$$

Note that the spectrum explicitly depends on the pump−probe delay T. Also, since the population in the ionic state remains constant after the ionization pulse stops, the states $|\psi_E\rangle$ at time $t = T$ (eq 5) enter in the expression for the spectrum. Thus, the subsequent time evolution in the ionic state does not influence the spectrum, which is important with respect to the wave packet imaging; see below.

The total ion yield, as a function of the pulse-delay, is calculated from the photoelectron spectrum by integration:

$$P_{\mathrm{tot}}(T) = \int \mathrm{d}E\, P(E, T) \tag{8}$$

Another measurable quantity is the momentum (p) distribution of the ionic fragments $F(p, T)$. This distribution can be calculated from the momentum-space wave functions of the states $|\psi_E(t)\rangle$ as

$$F(p, T) = \lim_{t\to\infty} \int \mathrm{d}E\, |\langle p|U_E(t - T)|\psi_E(T)\rangle|^2 = \int \mathrm{d}E\, |\langle p - |\psi_E(T)\rangle|^2 \tag{9}$$

The kets $|p-\rangle$ are the eigenstates of the full nuclear Hamiltonian and $|p\rangle$ are plane waves. It is important to notice that here the time-limit enters if the fragment distribution is calculated in terms of the projection on plane waves; i.e., a wave packet prepared at time T has to move into the asymptotic region in order to arrive at a constant momentum distribution.

3. Wave Packet Imaging

3.1. Transient Photoelectron Spectra. We start with the wave packet reconstruction from a given photoelectron spec-

trum. Therefore, an approximation to the equation for the ionic states $|\psi_E(T)\rangle$ is employed. The approximation consists of the neglect of commutators between the kinetic energy operators and the r-dependent operators (potential energy, dipole moment)[45−51] leading to

$$\psi_E(r,T) = \mu_{I1}(r)\, \psi_1(r,T)\, I(r,E) \tag{10}$$

with the integral

$$I(r,E) = \frac{i}{2} \int_{-\infty}^{\infty} \mathrm{d}t\, \mathrm{e}^{i(V_I(r)-V_1(r)-(\omega_2-E))t}\, g_2(t) \tag{11}$$

Here $V_n(r)$ denotes the potential energy in state $|n\rangle$. The photoelectron-spectrum now takes the form

$$P(E,T) = \int \mathrm{d}r\, \rho(r,T)\, |I(r,E)|^2 \tag{12}$$

where we used the definition for the density

$$\rho(r,T) = |\mu_{I1}(r)\, \psi_1(r,T)|^2 \tag{13}$$

It is the latter quantity that we want to reconstruct. From eq 12 it is clear that, to do so, a knowledge of the spectrum $P(E)$ and the function $I(r,E)$ is necessary. It is also obvious, that the product between the transition dipole moment and the vibrational wave function cannot be disentangled.

Let us now proceed to calculate the density from eq 12. As one possibility, the integral can be discretized, which leads to a matrix equation. The latter could, in principle, be inverted to yield the density. This approach was recently investigated by us in connection with the determination of dipole moments from time-resolved photoelectron spectra.[52] We will not discuss the method here. Instead, we evaluate the time-integral $I(r,E)$ employing a Gaussian envelope function as $g_2(t) = \exp(-(\beta t/2)^2)$ leading to the expression

$$I(r,E) = \frac{i}{2} \sqrt{4\pi/\beta^2}\, \mathrm{e}^{-(D(r)-(\omega_2-E))^2/\beta^2} \tag{14}$$

where we have introduced the difference potential $D(r) = V_I(r) - V_1(r)$. The function $I(r,E)$ represents a window function which is peaked around distances r_i which are the roots of the equation

$$D(r) - (\omega_2 - E) = 0 \tag{15}$$

Thus, for a monotonic difference potential (which is the case in our numerical example and will be assumed in what follows), the last equation establishes a clear connection between the bond length and the photoelectron energy. The window function becomes a representation of the δ-function in the limit of long pulses (i.e., for $\beta \rightarrow 0$). Thus, we may write

$$I(r,E) = i\pi\{\delta(D(r) - (\omega_2 - E)) + c(r,E)\} \tag{16}$$

where the additional term $c(r,E)$ compensates for the error made by replacing the window function by a δ-function. Neglecting the term $c(r,E)$ yields the spectrum in the simple form

$$P(E,T) \sim \frac{\rho(r_i,T)}{|\mathrm{d}D(r)/\mathrm{d}r|_{r_i}^2} \tag{17}$$

where we have used the property of the δ-function: $\delta(f(x)) = \delta(x)/|df/dx|_{x_i}$. This equation, together with eq 15, relates the radial probability density $\rho(r)$ and the photoelectron spectrum $P(E)$ for a fixed delay-time T. The approximations leading to eq 17, namely (a) the neglect of commutators of the potentials with the kinetic energy operator and (b) the replacement of the window function $I(r,E)$ by a δ-function, may be analyzed in detail.[47,53] Here we remark that for a constant difference potential, approximation (a) becomes exact, but then, the spectrum $P(E,T)$ is independent of the actual position of the wave function $\psi_1(r, T)$ (and consequently of time). Also, for a δ-pulse excitation, the spectrum becomes energy- and r-independent and no information can be gathered from the signal. On the other hand, for a very long pulse, the correction term $c(r,E)$ in eq 16 vanishes but then, approximation (a) is invalid. We thus expect that the connection formulated in eqs 16 and 17 is reasonable for substantially r-dependent difference potentials $D(r)$ and for pulses that are short compared to the vibrational periods but long enough to guarantee that the window function $I(r,E)$ is strongly peaked around the root of eq 15.

In the numerical examples given in section 3, the wave functions $|\psi_E(T)\rangle$ are calculated without further approximations from eq 5 and the photoelectron spectrum is obtained from the norm of these functions (eq 12). This spectrum is used as the input for the inversion; e.g., it plays the role of a data set which is taken from experiment. The density is obtained from eq 17 where the connection between energy and bond length is given via the resonance condition of eq 15.

3.2. Transient Ion Yields. In this subsection we discuss an imaging method which was first suggested in connection with pump−probe fluorescence signals.[23,24] Here, we briefly describe the idea and extend the method to experiments which measure transient ion yields. Figure 1 (middle panel) shows an ionization scheme, where the photon energy is chosen such that for a certain bond length $r = a$, it matches the difference potential, i.e., $\omega_2 = D(r = a)$. For delay-times T, when the wave packet $\psi_1(r,T)$ is located at distances r smaller than a, ionization is not possible. The ion yield increases if the packet moves into the region with $r \geq a$ and will eventually settle to a constant value. This happens, if the transition dipole moment μ_{I1} can be approximated by a constant and the laser frequency is large enough, for a detailed discussion; see refs 25, 54, and 55. Of course, for later times, the wave packet will pass the distance a on its way back and the signal again decreases to zero.

As in the last section we use a Gaussian probe−pulse to obtain the total ion yield as

$$P_{\mathrm{tot}}(T) = \frac{\pi}{\beta^2} \int \mathrm{d}r\, \rho(r,T) \int_0^{\infty} \mathrm{d}E\, \mathrm{e}^{-2[E-(\omega_2-D(r))]^2/\beta^2} \tag{18}$$

Performing the integration over energy and employing properties of the error function $\mathrm{erf}(x)$[56] yields

$$P_{\mathrm{tot}}(T) = \frac{(\pi/2)^{3/2}}{\beta} \int \mathrm{d}r\, \rho(r,T) \times \left\{1 + \mathrm{erf}\left[\frac{\sqrt{2}[\omega_2 - D(r)]}{\beta}\right]\right\} \tag{19}$$

The latter equation demonstrates in a clear way what has been said above: if the density $\rho(r,T)$ is located in a region where the argument of the error function is substantially negative, the signal is zero. If the wave packet moves into the region to the right of a, the signal levels off to a constant proportional to the area under the density, see the discussion in refs 24 and 56.

To establish the relation between the total ion yield at a fixed delay-time and the radial density, we replace the expression

$(1 + \mathrm{erf}(x))/2$ appearing in eq 19 by a step function $\Theta(r - a)$. It then can be shown that[23]

$$\frac{\mathrm{d}P_{\mathrm{tot}}(T)}{\mathrm{d}T} = j(a,T) \tag{20}$$

with $j(a,T)$ being the probability flux through the point $r = a$ at time T. Employing the definition

$$\mu_{I1}(r)\,\psi_1(r,T) = \sqrt{\rho(r,T)}\,\mathrm{e}^{iS(r,T)} \tag{21}$$

where $S(r,T)$ is a real function and assuming that the latter depends only weakly on the delay time, one finds

$$\frac{\mathrm{d}P_{\mathrm{tot}}(T)}{\mathrm{d}T} = \frac{1}{m}\left\{\frac{dS(r,T)}{\mathrm{d}r}\right\}_a \rho(a,T) \tag{22}$$

where m is the reduced mass. Thus, under the assumptions as made above, the time-derivative of the total ion signal is proportional to the density at the resonance point $r = a$ at time T.

In a last step, the density is constructed from the equation

$$\rho(r = a + \nu_0 t, T) \sim \left\{\frac{\mathrm{d}P(\lambda)}{\mathrm{d}\lambda}\right\}_{\lambda = T - t} \tag{23}$$

Here enters the average velocity of the wave packet motion in state $|1\rangle$ which can be estimated classically as $\nu_0 = \sqrt{2(\omega_1 - V_1(a))/m}$.

3.3. Transient Fragment Distributions. A third method for imaging wave packets was used before in the connection with the Coulomb explosion of small molecules.[31−33] A critical analysis of this method was given by Chelkowski and Bandrauk.[33] The main idea here is to relate the asymptotic momentum distribution of the atomic ions to the density $\rho(r,T)$ at the time T that the ionization proceeds; see Figure 1, lower panel.

Inserting eq 5 into the expression for the fragment distribution (eq 9) yields:

$$F(p,T) = \int \mathrm{d}E \left| \int \mathrm{d}r\, \langle p - |r\rangle \right.$$
$$\left. \langle r | \int \mathrm{d}t\, \mathrm{e}^{i(p^2/2m + V_I(\infty) + E - \omega_2 - V_1)t}\, \frac{i}{2}\, g_2(t)\, \mu_{I1}\, \psi_1(T)\rangle \right|^2 \tag{24}$$

where we used the fact that $|p-\rangle$ is an eigenstate of the Hamiltonian in the ionic state and neglected the kinetic energy operator in state $|1\rangle$. Employing, as in the preceding sections, a Gaussian for the probe−pulse envelope, the time integral can be evaluated as

$$I_p(r,E) = \frac{i}{2}\int_{-\infty}^{\infty} \mathrm{d}t\, \mathrm{e}^{i(p^2/2m + V_I(\infty) - V_1(r) - (\omega_2 - E))t}\, g_2(t) \tag{25}$$

$$= \frac{i}{2}\sqrt{4\pi/\beta^2}\, \mathrm{e}^{-(p^2/2m + V_I(\infty) - V_1(r) - (\omega_2 - E))^2/\beta^2} \tag{26}$$

Following the arguments as given in section 3.1, the window function is written as

$$I_p(r,E) =$$
$$i\pi\left\{\delta\left(\frac{p^2}{2m} + V_I(\infty) - V_1(r) - (\omega_2 - E)\right) + c_p(r,E)\right\} \tag{27}$$

The latter function is now replaced by a δ-function as

$$I_p(r,E) = i\pi\left\{\delta\left(\frac{p^2}{2m} + V_I(\infty) - V_1(r) - (\omega_2 - E)\right)\right\} =$$
$$i\pi\frac{\delta(r - r_i)}{|dV_1(r)/\mathrm{d}r|_{r_i}} \tag{28}$$

Here, the values r_i are obtained as roots of the equation

$$\frac{p^2}{2m} + V_I(\infty) - V_1(r) - (\omega_2 - E) = 0 \tag{29}$$

Note that, since we have used a projection on the eigenstate $|p-\rangle$ to calculate the fragment distribution, the value of the momentum p is fixed so that r depends only parametrically on p. Evaluating the integral over r leads to the fragment distribution

$$F(p,T) \sim \int \mathrm{d}E\, \frac{|\langle p - |r_i(E)\rangle|^2 \rho(r_i(E),T)}{|dV_1(r)/\mathrm{d}r|^2_{r_i(\mathrm{E})}} \tag{30}$$

To eliminate the integral over energy, an additional approximation is introduced. Therefore, although the probe pulse is spectrally broad, we employ the limit of energy conservation which says that, at a given value of r, we must have (see Figure 1, lower panel)

$$V_1(r) + \omega_2 = V_I(r) + E \tag{31}$$

This allows one to eliminate the photoelectron energy from eq 29 to obtain

$$\frac{p^2}{2m} + V_I(\infty) - V_I(r) = 0 \tag{32}$$

Since the roots r_i, as determined from the latter equation, are independent of E, the momentum distribution now reads

$$F(p,T) \sim \frac{|\langle p - |r_i\rangle|^2\, \rho(r_i,T)}{|\mathrm{d}V_1(r)/\mathrm{d}r|^2_{r_i}} \tag{33}$$

In principle, for a given potential $V_I(r)$, the stationary scattering states $\langle p - |r\rangle$ can be calculated by solving

$$\left\{\frac{\hat{p}^2}{2m} + V_I\right\}|p-\rangle = \left(\frac{p^2}{2m} + V_I(\infty)\right)|p-\rangle \tag{34}$$

taking the proper boundary conditions into account. Within a linear approximation to the potential around the point r_i, the solution of the time-independent Schrödinger equation is an Airy function $Ai(r = r_i) = Ai(0)$, thus is independent of r_i [12] and may be omitted in evaluating the fragment distribution. The final expression then is

$$F(p_i,T) \sim \frac{\rho(r_i,T)}{|\mathrm{d}V_1(r)/\mathrm{d}r|^2_{r_i}} \tag{35}$$

The expression for the photofragment (eq 35) and photoelectron spectrum (eq 17) are very similar and are identical if the denominators (containing the derivative of $V_1(r)$ and $D(r)$ at the same resonance distance) are set to the same constant. They are, however, based on different kind of approximations.

In practice, the momentum distributions are calculated from eq 9: for a fixed value of E we propagate the wave functions

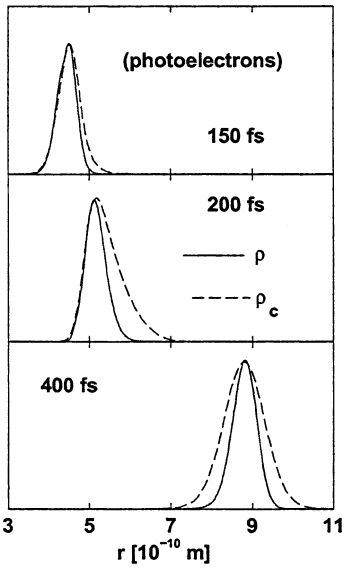

Figure 2. Constructed (ρ_c) vs numerically exact density ρ for different pump−probe delays. The densities are derived from the photoelectron spectra.

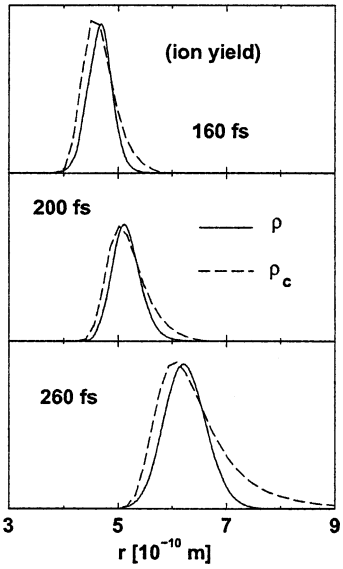

Figure 3. Constructed (ρ_c) vs numerically exact density ρ for different pump−probe delays. Here the wave packet imaging is performed using the time-derivative of the transient ion yield. The choice of the probe photon energies allows for the mapping at different bond lengths. The numbers given in the different panels indicate the times when the wave packet has completely entered the excitation window so that the ionization signal has leveled to a constant.

$\psi_E(r,T)$ until they are completely localized in the asymptotic region. Then the coordinate space wave function is transformed into momentum space. This is repeated for a discrete set of energies E which covers the photoelectron spectrum sufficiently. Finally, the energy integral is calculated. The thus obtained distributions which represent the experimentally provided input, then enter into eq 35 to determine the density $\rho(r_i)$, where the distances r_i fulfill eq 32.

4. Numerical Examples

First, the construction of radial densities from photoelectron spectra will be treated. In what follows, results are discussed for photon energies of 3.73 eV (pump−pulse) and 4.5 eV (probe−pulse). The Gaussian pump pulse had a duration of 50 fs (full width at half-maximum), and a shorter (Gaussian) probe−pulse of 20 fs was employed. Figure 2 compares the numerically exact density $\rho(r,T)$ with the constructed density $\rho_c(r,T)$ obtained from eq 17 for different delay-times T, as indicated. In our case, the difference potential between the double-minimum state $|1\rangle$ and the repulsive ionic state $|I\rangle$ is a monotonicly decreasing function of r (in the region, the vibrational wave packet dynamics takes place), so that there is a one-to-one correspondence between the points r_i and the photoelectron energy, as defined via the equality in eq 15. The figure documents that the prescription for the construction of the density is indeed excellent, as was demonstrated theoretically before.[57,58] For all three delay times, the position of the maximum of $\rho_c(r)$ coincides with that of $\rho(r)$. Also, the widths of the densities agree well so that here we may say that wave packet imaging through time-resolved photoelectron spectroscopy works very well.

Next, we turn to the densities, as obtained from the total ion yields using eq 23. The same parameters for the pulses as specified above were used except that the probe photon-energy was varied. As is sketched in Figure 1, resonant ionization with pulses of different photon energies ω_2 selects different bond lengths $r = a$, at which the vibrational wave packet can be monitored. Figure 3 contains the calculated densities. We chose ω_2 to assume values of 3.1 eV (upper panel), 2.95 eV (middle panel), and 2.76 eV (lower panel), corresponding to bond lengths of $a = 4.3$, 4.6, and 5.0 Å, respectively. For the choice of the first two parameters, the constructed and numerically exact densities agree perfectly. A larger discrepancy occurs in the $a = 5.0$ Å case, mainly at longer bond lengths. This has to do with the fact that here the wave packet passes the barrier of the double minimum state and thus the approximation of a constant velocity v_0 within this state is not valid. It has to be noted that a wave packet being localized in the regions of the classical turning points in the potential $V_1(r)$ cannot be monitored using the flux method as described above, since the transient ion yield will not level to a constant value as a function of delay time.

Finally, we discuss the wave packet imaging by inversion of the fragment distribution. As in the case of the photoelectron spectra pulses with $\omega_1 = 3.73$ eV, 50 fs width (pump) and $\omega_2 = 4.5$ eV, 20 fs width (probe) were employed. The upper panel of Figure 4 compares the densities at a delay-time of $T = 100$ fs. Here, the vibrational wave packet in the intermediate state is localized at a bond length between 3 and 4 Å. The constructed density is shifted slightly toward smaller distances as compared to the numerically exact one. At a later time of 150 fs, the fact that ρ_c peaks at smaller distance is as well observed. This trend continues and is most pronounced at $T = 250$ fs (lower panel of Figure 4). The reason for the discrepancy in the location of the two densities can be rationalized in the following way: the basic idea of the construction method is that the initial wave packet, produced within the ionization step, carries a momentum distribution which is dominated by components with zero momentum, and thus the energy at early times is almost exclusively potential energy. The latter then is transformed into kinetic energy of the fragments. The assumption of a mean zero momentum is not necessarily valid: since the wave packet $\psi_1(r, T)$ is moving outward in the double-minimum state, its kinetic energy is transferred into the ionic state (see, e.g., eq 10). Thus, the fragment distribution peaks at a higher momentum which, in turn, yields a constructed density at shorter distances. This reasoning also explains why the mismatch in the peak position increases in going from 100 to 250 fs since for the longer time, the lower state wave packet has picked up more speed.

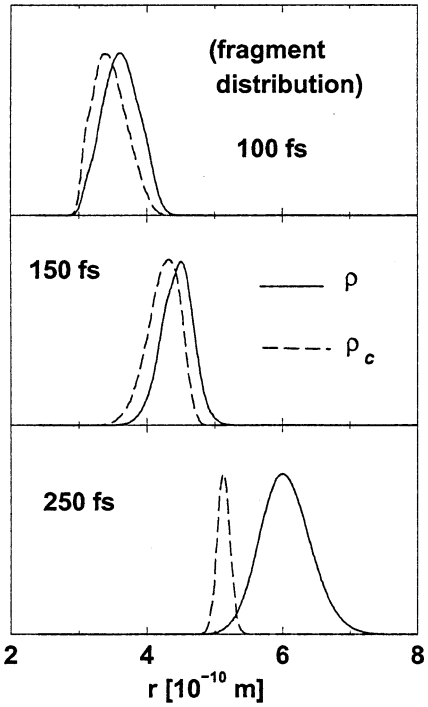

Figure 4. Constructed (ρ_c) vs numerically exact density ρ for different pump−probe delays. The momentum distribution of the fragments was used for the construction.

As a second observation the deviation in the width of the two densities is much more pronounced in the 250 fs case than at earlier times. Because of the large positive momentum from the intermediate state dynamics, the fragment momentum distribution yields a constructed density at too small distances where the potential energy is rather steep and thus the width becomes too small as well.

Altogether, for the example regarded here, the use of the fragment distribution is good as long as the vibrational wave packet in state $|1\rangle$ has not developed a momentum distribution far away from zero momentum which, in the present example, is the case at small delay times. The imaging procedure could be improved in a simple way if additional information about the kinetic energy in the intermediate state are available.[33]

5. Summary

Three methods to image the density of vibrational wave packets have been discussed. They are based on a pump−probe ionization scheme employing ultrashort laser pulses. In the first method, the photoelectron spectrum is used for the construction of the density. Because of the very fast ejection of the photoelectron an excellent snapshot of the density at the time of the ionization is obtained. The subsequent dynamics in the ionic state, leading to a modification of the wave packet does not enter into the signal. Extending our former work on pump−probe fluorescence spectroscopy, we showed that transient ion yields can be used to map vibrational densities. The underlying method does also yield reliable results in the present case, but is of lower quality for a flat difference potential between the neutral and ionic state. Opposite to the time-resolved photoelectron measurements, here it is necessary to adjust the probe−pulse wavelength in order to map the wave packet at different times (distances). As a third method, we investigated photofragment distributions which, using energy conservation arguments, can be related to the vibrational densities. The quality of the procedure depends more critically on the location of the wave packet in comparison to the results as obtained using the other two methods. It should be noted that in all three cases essentially the same approximation were involved leading to a simple physical picture relating wave functions and observables. It is of course possible to implement corrections (see, e.g., ref 33) to the approximations, but owing to limited experimental resolution this might not be useful. In conclusion, we have demonstrated that pump−probe ionization experiments are well suited to characterize vibrational wave packets in small molecules and to monitor their temporal changes.

Acknowledgment. We gratefully acknowledge support by the NRC-Helmholtz Program, the DTU Visiting Scientist Program (project ADAM), and the Fonds der Chemischen Industrie.

References and Notes

(1) Garraway, B. M.; Suominen, K.-A. *Rep. Prog. Phys.* **1995**, *58*, 365.
(2) Yeazell, J.; Uzer, T. *The Physics and Chemistry of Wave Packets*; Wiley: New York, 2000.
(3) Baumert, T.; Gerber, G. *Adv. At. Mol. Opt. Phys.* **1995**, *35*, 163.
(4) Baumert, T.; Herek, J. L.; Zewail, A. H. *J. Chem. Phys.* **1993**, *99*, 4430.
(5) Berry, R. S.; Bonacic-Koutecky, V.; Gaus, J.; Leisner, T.; Manz, J.; Reischl-Lenz, B.; Ruppe, H.; Rutz, S.; Schreiber, E.; Vajda, S.; de Vivie-Riedle, R.; Wolf, S.; Wöste, L. *Adv. Chem. Phys.* **1997**, *101*, 101.
(6) Schwoerer, H.; Pausch, R.; Heid, M.; Engel, V.; Kiefer, W. *J. Chem. Phys.* **1997**, *107*, 9749.
(7) Neumark, D. M. *Annu. Rev. Phys. Chem.* **2001**, *52*, 255.
(8) Stolow, A. *Int. Rev. Phys. Chem.* **2003**, *22*, 377.
(9) Stolow, A. *Annu. Rev. Phys. Chem.* **2003**, *54*, 89.
(10) Herzberg, G. *Spectra of Diatomic Molecules*; van Nostrand Reinhold: New York, 1950.
(11) Tellinguisen, J. In *Photodissociation and Photoionization*, 3rd ed.; Wiley: New York, 1985.
(12) Schinke, R. *Photodissociation Dynamics*; Cambridge University Press: Cambridge, England, 1993.
(13) Rost, J. M. *J. Phys. B: At. Mol. Opt. Phys.* **1995**, *28*, L601.
(14) Kolba, E.; Manz, J.; Schreier, H. J.; Trisca, I. *Chem. Phys. Lett.* **1992**, *189*, 505.
(15) Vogt, P.; Schmitt, M.; Kiefer, W. *Chem. Phys. Lett.* **1995**, *243*, 64.
(16) Lee, S. Y. *Chem. Phys. Lett.* **1993**, *203*, 93.
(17) Eichelsdörfer, M.; Engel, V. *Chem. Phys. Lett.* **1996**, *263*, 640.
(18) Schinke, R. J. *Chem. Phys.* **1986**, *85*, 5049.
(19) Hennig, S.; Engel, V.; Schinke, R. *J. Chem. Phys.* **1986**, *84*, 5444.
(20) Eberly, J. H.; Wodkiewicz, K. *J. Opt. Soc. Am.* **1977**, *67*, 1252.
(21) Dunn, T. J.; Sweetser, J. N.; Walmsley, I. A.; Radzewicz, C. *Phys. Rev. Lett.* **1995**, *74*, 884.
(22) Dunn, T. J.; Walmsley, I. A.; Mukamel, S. *Phys. Rev. Lett.* **1995**, *74*, 884.
(23) Engel, V.; Henriksen, N. E. *J. Chem. Phys.* **2000**, *112*, 106.
(24) Henriksen, N. E.; Engel, V. *Int. Rev. Phys. Chem.* **2001**, *20*, 93.
(25) Seel, M.; Domcke, W. *Chem. Phys.* **1991**, *151*, 59.
(26) Seel, M.; Domcke, W. *J. Chem. Phys.* **1991**, *95*, 7806.
(27) Meier, C.; Engel, V. *Chem. Phys. Lett.* **1993**, *212*, 691.
(28) Assion, A.; Geisler, M.; Helbing, J.; Seyfried, V.; Baumert, T. *Phys. Rev. A* **1996**, *54*, R4605.
(29) Frohnmeyer, T.; Hofmann, M.; Strehle, M.; Baumert, T. *Chem. Phys. Lett.* **1999**, *312*, 447.
(30) Frohnmeyer, T.; Baumert, T. *Appl. Phys. B* **2000**, *71*, 259.
(31) Stapelfeldt, H.; Constant, E.; Sakai, H.; Corkum, P. B. *Phys. Rev. A* **1998**, *58*, 426.
(32) Bandrauk, A. D.; Chelkowski, S. *Phys. Rev. Lett.* **2001**, *87*, 273004.
(33) Chelkowski, S.; Bandrauk, A. D. *Phys. Rev. A* **2002**, *65*, 023403.
(34) Assion, A.; Baumert, T.; Geisler, M.; Seyfried, V.; Gerber, G. *Euro. Phys. J. D* **1998**, *4*, 145.
(35) Skovsen, E.; Machholm, M.; Ejdrup, T.; Thøgersen, J.; Stapelfeldt, H. *Phys. Rev. Lett.* **2002**, *89*, 133004.
(36) Leonard, U.; Raymer, M. G. *Phys. Rev. Lett.* **1995**, *76*, 1985.
(37) Leichtle, C.; Schleich, W. P.; Averbukh, I. S.; Shapiro, M. *Phys. Rev. Lett.* **1998**, *80*, 1418.
(38) Weinacht, T. C.; Ahn, J.; Bucksbaum, P. H. *Phys. Rev. Lett.* **1998**, *80*, 5508.
(39) Lein, M.; Erdmann, M.; Engel, V. *J. Chem. Phys.* **2000**, *113*, 3609.
(40) Skovsen, E.; Stapelfeldt, H.; Juhl, S.; Mølmer, K. *Phys. Rev. A* **1998**, *58*, 426.
(41) Baumert, T.; Gerber, G. *Isr. J. Chem.* **1994**, *34*, 103.
(42) Assion, A.; Baumert, T.; Seyfried, V.; Weiss, V.; Wiedenmann, E.; Gerber, G. *Z. Phys. D: At., Mol. Clusters* **1996**, *36*, 265.

(43) Wollenhaupt, M.; Assion, A.; Bazhan, O.; Horn, C.; Liese, D.; Sarpe-Tudoran, C.; Winter, M.; Baumert, T. *Chem. Phys. Lett.* **2003**, *376*, 457.
(44) Feit, M. D.; Fleck, J. A.; Steiger, A. J. *Comput. Phys.* **1982**, *47*, 412.
(45) Lax, M. J. *Chem. Phys.* **1952**, *20*, 1752.
(46) Lee, S.-Y.; Pollard, W. T.; Mathies, R. A. *Chem. Phys. Lett.* **1989**, *163*, 11.
(47) Braun, M.; Meier, C.; Engel, V. *J. Chem. Phys.* **1995**, *103*, 7907.
(48) Li, Z.; Fang, J.-Y.; Martens, C. C. *J. Chem. Phys.* **1996**, *104*, 6919.
(49) Hiller, E. M.; Cina, J. A. J. *Chem. Phys.* **1996**, *105*, 3419.
(50) Cao, J.; Wilson, K. R. *J. Chem. Phys.* **1997**, *106*, 5062.
(51) Dilthey, S.; Hahn, S.; Stock, G. *J. Chem. Phys.* **2000**, *112*, 4910.
(52) Lohmüller, T.; Erdmann, M.; Rubner, O.; Engel, V. *Eur. Phys. J. D* **2003**, *25*, 95.
(53) Ermoshin, V. A.; Engel, V. *Eur. Phys. J. D* **2001**, *15*, 413.
(54) Engel, V. *Chem. Phys. Lett.* **1991**, *178*, 130.
(55) Lohmüller, T.; Erdmann, M.; Engel, V. *Chem. Phys. Lett.* **2003**, *373*, 319.
(56) Henriksen, N. *E. Adv. Chem. Phys.* **1995**, *91*, 433.
(57) Shen, Z.; Boustani, I.; Erdmann, M.; Engel, V. *Chem. Phys. Lett.* **2001**, *339*, 362.
(58) Shen, Z.; Engel, V. *Chem. Phys. Lett.* **2002**, *358*, 344.